Micro-scale to Meso-scale Analysis of Parenchymal Tethering: The Effect of
Heterogeneous Alveolar Pressures on the Pulmonary Mechanics of Compliant Airways

Jason Ryans¹, Hideki Fujioka², Donald P. Gaver¹

¹Department of Biomedical Engineering, Tulane University, New Orleans, LA, USA

²Technology Services and Center for Computational Science, Tulane University, New Orleans,

LA, USA

Correspondence: Donald P. Gaver

(E) dpg@tulane.edu

(T) 504-865-5150

534 Lindy Boggs

Department of Biomedical Engineering

Tulane University

New Orleans, LA 70118

Abstract

In the healthy lung, bronchi are tethered open by the surrounding parenchyma; for a uniform distribution of these peri-bronchial structures, the solution is well known. An open question remains regarding the effect of a distributed set of collapsed alveoli, as can occur in disease. Here we address this question by developing and analyzing micro-scale finite-element models of systems of heterogeneously inflated alveoli to determine the range and extent of parenchymal tethering effects on a neighboring collapsible airway. This analysis demonstrates that micromechanical stresses extend over a range of approximately 5 airway radii, and this behavior is dictated primarily by the fraction, not distribution, of collapsed alveoli in that region. A meso-scale analysis of the micro-scale data identifies an effective shear modulus, G_{eff} , that accurately characterizes the parenchymal support as a function of the average transpulmonary pressure of the surrounding alveoli. We demonstrate the use of this formulation by analyzing a simple model of a single collapsible airway surrounded by heterogeneously inflated alveoli (a 'pig-in-a-blanket' model), which quantitatively demonstrates the increased parenchymal compliance and reduction in airway caliber that occurs with decreased parenchymal support from hypo-inflated obstructed alveoli. This study provides a building block from which models of an entire lung can be developed in a computationally tenable manner that would simulate heterogeneous pulmonary mechanical interdependence. Such multi-scale models could provide fundamental insight towards the development of protective ventilation strategies to reduce the incidence or severity of ventilator-induced lung injury, VILI.

New & Noteworthy

A destabilized lung leads to airway and alveolar collapse that can result in catastrophic pulmonary failure. This study elucidates the micromechanical effects of alveolar collapse and determines its range of influence on neighboring collapsible airways. A meso-scale analysis reveals a master relationship that can that can be used, in a computationally efficient manner, to quantitatively model alveolar mechanical heterogeneity that exists in acute respiratory distress syndrome (ARDS), which predisposes the lung to volutrauma and/or atelectrauma. This analysis may lead to computationally tenable simulations of heterogeneous organ-level mechanical interactions that can illuminate novel protective ventilation strategies to reduce VILI.

Keywords: Shear modulus, parenchymal tethering, reduced-dimension model, acute respiratory distress syndrome, mechanical ventilation

1. Introduction

The mammalian lung is an extraordinary example of a physiological organ whose function depends upon microfluidic principles. Despite its high mechanical compliance, the healthy lung is remarkably stable because of two interdependent mechanical processes:

- Mechanical interdependency exists between the alveoli and airways, with the alveoli functioning as a foam-like structure that provides parenchymal tethering support of compliant airways, and
- 2) Pulmonary surfactant physicochemical properties reduce and dynamically modify the lining fluid surface tension during respiration. This stabilizes the lung by modifying the elastic recoil as a function of the history of interfacial expansion/compression (18), and counteracts the interfacial instabilities that can lead to airway and alveolar obstructions that would reduce gas exchange.

These two effects are linked, because surface tension modulates parenchymal tethering and can influence airway stability from fluid-structure interactions related to the Plateau-Rayleigh instability (9-11, 14, 15). This, in turn, can detrimentally affect gas-flow to the subtended alveoli, further reducing parenchymal tethering with potentially devastating effects. These are prime examples of multi-scale interactions that span from the molecular-scale (surfactant), to subsubmillimeter-scale (single- and multi-cellular) to millimeter-scale (alveolar) mechanical interactions. Thus, small-scale interactions function in concert to stabilize the large-scale organ.

Parenchymal tethering plays a crucial role in maintaining airway patency (17, 25, 31). Lai-Fook et al.(19) investigated the mechanical interdependency between bronchial pressure-volume behavior and the parenchyma shear modulus (G) as a function of the transpulmonary pressure (P_{TP}) in a uniformly inflated lung. That study demonstrates that increasing the lung volume significantly increases the peri-bronchial stress, which helps to sustain airway patency and stabilize the lung. Positive-end-expiratory-pressure (PEEP) ventilation is a useful protocol that takes advantage of this principle to maintain lung stability.

Unfortunately, in acute respiratory distress syndrome (ARDS), pulmonary stability can break down. Liquid obstruction of airways impairs gas exchange and results in heterogeneous ventilation. Ventilator-induced lung injury (VILI) can occur from either over-distension

(volutrauma) or repetitive closing and reopening of compliant airways and alveoli (atelectrauma) (12), though recent studies indicate that atelectrauma predisposes the lung to volutrauma(13).

Venegas and Winkler *et al.*(29) developed a network model of airway/parenchyma interactions that suggests that the progression of poorly ventilated regions increase catastrophically if local tethering is heterogeneous. Clearly, then, heterogeneous tethering should be included in any multi-scale lung model if one intends to simulate the abnormal pulmonary mechanical phenomena associated with ARDS. Organ-level models that could investigate the full repertoire of patho-physiological micro-scale (alveolar-level) and macro-scale (lobular and full-organ) interactions would require computations of the interactions of over 10⁸ alveoli and associated airways in a 3-d compliant structure with heterogeneity due to lung geometry, gravity, tissue properties, and disease progression. This approach is simply untenable with today's computing environments; nevertheless, if possible these simulations could forecast protective modes of ventilation that could reduce VILI.

While a complete organ-level multiscale model of the lung is not feasible, we hypothesize that it is possible to develop insight from micro-scale models that, with appropriate volume averaging, can reveal meso-scale properties that can create the link between small- and large-scale structures. At the micro-scale, Denny *et al.*(3) and Fujioka *et al.*(6) developed finite element models (FEM) of connected, compartmentalized alveoli to elucidate the mechanical properties of lung parenchyma under a variety of mechanical loading scenarios. We seek to extend these models to the meso-scale, which reflects the parenchymal tethering effects relevant to an airway. This is an important step in creating multi-scale models of the entire lung.

Therefore, in the present study we explore FEM models associated with obstructed and unobstructed alveoli in the neighborhood of a compliant airway to establish the mechanical properties that affect the peri-bronchial stress that influence airway stability under pathophysiological conditions. We use this highly detailed micro-scale FEM model to provide data from which we establish an equivalent meso-scale continuum mechanics construct, the

effective shear modulus (G_{eff}), that can faithfully represent the influence of heterogeneously obstructed alveoli and their effect on parenchymal tethering of compliant pulmonary airways. This goal is a critical step towards the development of a computationally tractable multi-scale model of the full lung that uses first-principles to simulate pulmonary mechanical interactions.

Conceptual Framework

Parenchyma is modeled by a 3-d network of interacting micro-scale alveoli surrounding an airway. The alveolar model is based upon Fujioka *et al*(6), and is simulated using high performance computing (HPC) approaches, from which the physical relationships are derived following Fujioka et al(7). We focus on identifying parenchymal tethering effects of non-uniformly recruited alveoli surrounding a small compliant airway, since these interactions influence organlevel behavior. We seek to re-express key results in a reduced-dimension parametric formulation that is deduced from a rational mechanics analysis of the meso-scale system. If successful, such a formulation could be used to accurately simulate the complex mechanical interactions within the lung using a strategy following Ryans *et al* (27).

To establish the reduced-dimension empirical relationships, we utilize FEM models to investigate the mechanical relationship between the airway and its surrounding parenchyma. We then define the equivalent interactions in a continuum mechanics framework, from which we estimate G_{eff} . For instance, consider the scenario illustrated in Figure 1, where an airway obstruction results in the presence of obstructed (red) alveoli with other patent pathways leading to aerated (blue) alveoli surrounding an airway.

We assume that the obstructed alveoli are air-filled, but remain inflated with a pressure, P_{OBS} , that deviates from aerated alveoli, $(P_{ALV})_{open}$. $P_{OBS} \neq (P_{ALV})_{open}$ because the obstruction acts as a pressure-relief valve due to a yield-pressure phenomenon wherein the liquid blockage moves only if a critical pressure drop (P_{yield}) is exceeded (8, 26, 32). In the analysis that follows,

we assume that $P_{yield} = 8\gamma/R = 4$ cmH₂0, as would be appropriate for the closure of a 1mm diameter airway with surface tension $\gamma = 25$ mN/m.

We investigate systems with either

- a) hypo-inflated obstructed alveoli ($P_{OBS} = (P_{ALV})_{open} P_{yield}$) that would occur when airway closure occurs at end-expiration, or
- b) hyper-inflated obstructed alveoli ($P_{OBS} = (P_{ALV})_{open} + P_{yield}$) that can occur due to the elastic recoil of the obstructed alveolus leading to an increase in the gas pressure within the obstructed alveolus.

In all cases we assume that the obstructed alveolus remains gas-filled from tethering effects of neighboring alveoli, and neglect absorption atelectasis.

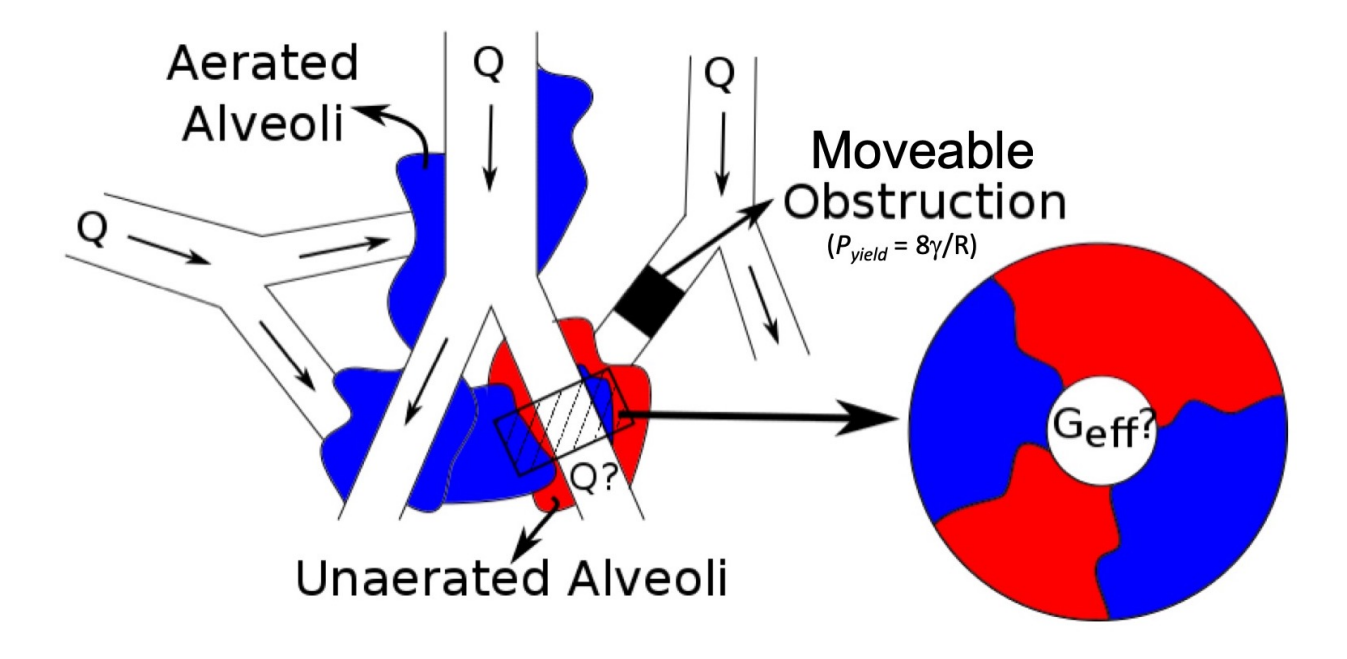


Figure 1: Representative illustration of airway obstruction resulting in the presence of aerated (**blue**) and obstructed (**red**) alveoli surrounding separate conducting airways.

The cross-sectional view in Figure 1represents the distribution of aerated and obstructed alveoli surrounding the airway – this distribution results in regions with significantly different alveolar pressures that can heterogeneously influence airway tethering. From this discrete

representation, we seek a continuum model that can represent the relationship between the peri-bronchial pressure exerted on the airway by the parenchyma, and the inflation states of the alveoli. To do so, we seek to establish the relationship between the effective shear modulus (G_{eff}) defined in Eqn (1) below, and the alveolar pressure distribution.

Clearly many permutations of the heterogeneous alveolar distribution exist, and it is not feasible to create a model to account for every scenario. In lieu of that, we investigate statistical variations of this distribution (Figure 2) by assuming that obstructed alveoli are randomly dispersed within the parenchyma while retaining the ratio of obstructed/unobstructed alveoli (the 'sprinkled donut' model).

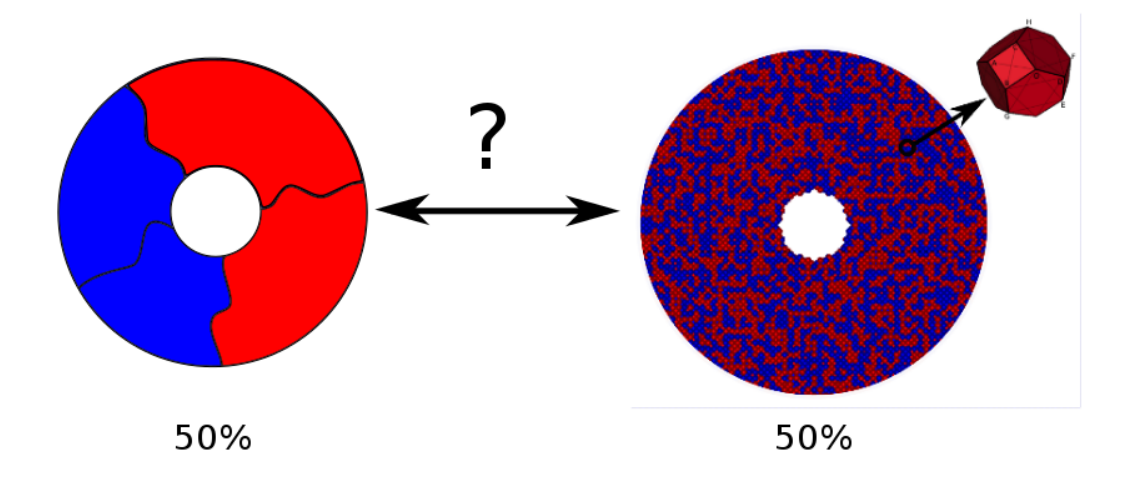


Figure 2: Approximation of heterogeneous tethering using a uniformly random distribution of obstructed alveoli ('sprinkled donut').

Computational experiments are conducted with these random distributions to identify the relationships between G_{eff} of the parenchyma, the percentage of impaired alveoli present, and the sensitivity of G_{eff} to the distribution of collapsed alveoli. We seek to answer two questions:

- 1. What region of influence surrounding the airway (R_{ROI}) determines the relevant effective shear modulus of the surrounding parenchyma?
- 2. Is the effective shear modulus with a uniform random distribution of closed alveoli equivalent mechanically to the effective shear modulus with localized regions of closure if the same fractions of alveoli are collapsed?

If we can identify a suitable R_{ROI} , and if we find that G_{eff} is only a function of the fraction of collapsed alveoli (insensitive to the distribution), we can then be confident that an empirical relationship of this meso-scale representation of the parenchymal mechanics can provide the foundation for a reduced-dimension model that can be efficiently implemented to model airway/parenchymal interactions in the entire lung.

2. Methods

2.1. The Finite-Element Model

We investigate an annular region of parenchyma surrounding a cylindrical "hole" following the work of Lai-Fook et al.(20) This investigation will elucidate the mechanical properties of the parenchyma alone, and further analysis (*Discussion*) will incorporate these results into the periairway pressure component of the transmural pressure for a compliant airway.

Our analysis is based upon a finite element model (FEM) that was developed to establish the relationship between the effective shear modulus (G_{eff}) of parenchyma surrounding an airway, and the transpulmonary pressures of the corresponding alveoli (6). In that model, the lung parenchyma is comprised of individual alveolar chambers modeled by truncated octahedrons. This displacement-based FEM model is utilized to analyze the deformations of the alveolar system as a function of the pressure in each alveolus, the outer pressure, and the fiber constitutive relationships.

Each face consists of septal border fiber bundles that lie on the perimeter of the face and cross-linking fiber bundles that lie across the face. Each alveolus sustains the force balance through elastin and collagen fibers arranged on the alveolar membrane – these membranes are under tension from neighboring elements and a pressure-difference across the membrane, providing a normal-stress on the membrane. A thin surfactant-laden liquid layer exists in the alveolus where the surface tension (γ) is a function of the interfacial surfactant concentration (Γ).

To model the effect of surface tension, we consider a sphere of the same volume as the truncated octahedron model of the alveolus (see Figure 2), V_{alv} , and define the radius of the equivalent sphere to be $R_{alv} = (3V_{alv}/4\pi)^{1/3}$. The pressure jump across the liquid lining is assumed to be $\Delta P = 2\gamma/R_{alv}$. Assuming a uniform surfactant concentration, $\Gamma = M_{ALV}/S_{ALV}$, where M_{ALV} is the mass of surfactant, and S_{ALV} is the surface area of an alveolus. A linear equation of state is used to calculate $\gamma(\Gamma)$, with M_{ALV} and the slope of the equation of state determined such that $\gamma = 30 \ dyn/cm$ at TLC, and $\gamma = 5 \ dyn/cm$ at TLC/3.

The boundary conditions for the FEM annulus surrounding the parenchymal hole allow the alveolar elements to expand and contract freely. This is accomplished by defining the stresses at the faces of the domain as illustrated in Figure 3, where the boundaries support zero tangential stresses. Each face has a normal stress/strain conditions where the fixed face (red) of the annulus restricts movement in the positive z-direction ($u_z = 0$), along the cylindrical face (blue), the normal stress is the negative of the surrounding pleural pressure ($\tau_{rr} = -P_{PL}$), and the opposing free-moving face (green) has normal stress $\tau_{zz} = -P_{PL}$. The hole is external to the domain of the finite-element model, and provides stress to the parenchyma through application of P_{PA} (see Figure 4).

Simulations proceed to mechanical equilibrium at the micro-scale by varying the nodal positions until $\sum \delta F < 10^{-5} dyn$ at each node, where $\delta F = F_p - F_f$, with F_p representing the equivalent vertex forces due to the pressures and F_f are the forces resulted from the extension of fibers.

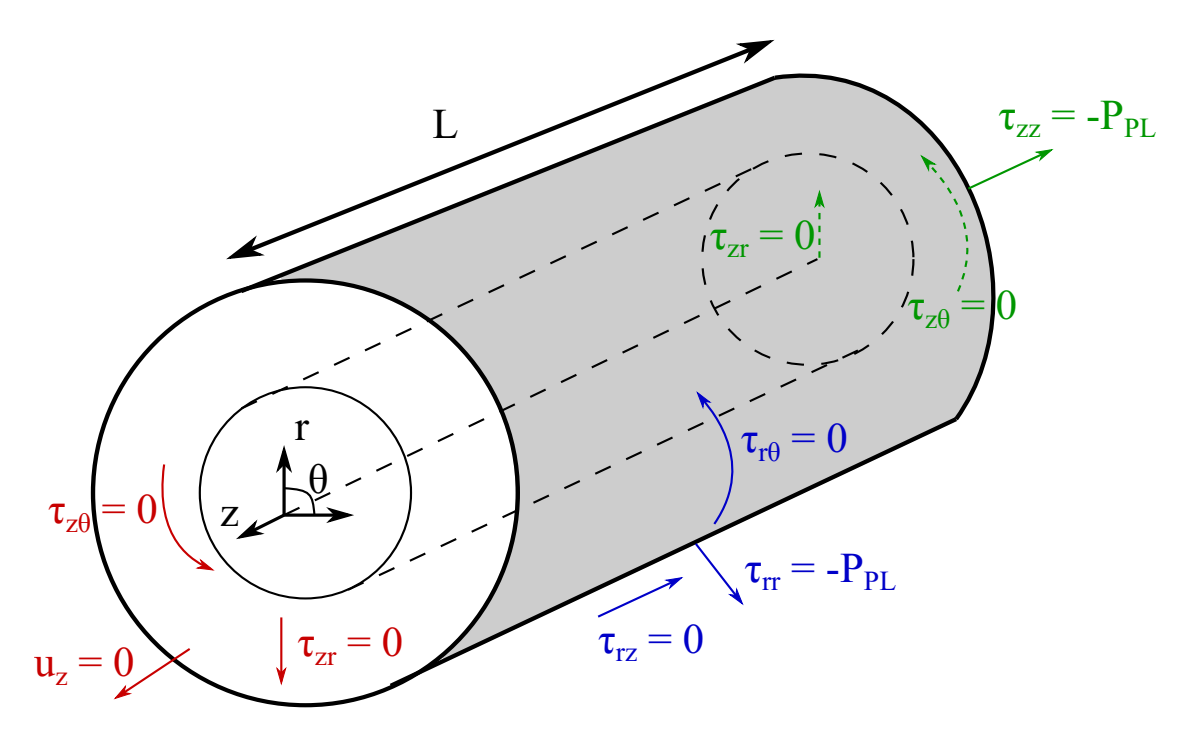


Figure 3: Boundary conditions of FEM model on the fixed face (**red**), cylindrical face (**blue**), and free-moving face (**green**). The interior hole is assumed to be at a constant pressure (P_{PA}) as shown in Figure 4.

We investigate perturbations from this state to identify meso-scale characteristics (G_{eff}) that describe the mechanical features of non-uniformly inflated alveoli as a function of the mean transpulmonary pressure following Wilson (30). Deformations are computed for the parenchyma as alveolar pressures are modified to represent inflation, deflation or upstream closure. As we will show below, perturbations of the peri-airway pressure (P_{PA}) induce modifications of a parenchymal hole lumen cross-sectional area, and this deformation provides the data necessary to identify G_{eff} . We use this process to calculate G_{eff} from both localized and random distributions of obstructed alveoli.

2.2. Model Mechanics

Model mechanics are driven by the interactions between the adjoining alveoli and the distending peri-airway pressure (P_{PA}) induced in the model. The airway-parenchyma model shown in Figure 3 and Figure 4 depict a collection of alveoli surrounding a hole in the

parenchyma. The effective shear modulus (G_{eff}) is analyzed following the analytical formulation for changes in radius for infinitely long cylindrical tubes in a homogeneous isotropic material as

$$\frac{\Delta R}{R} = \frac{P_{PA} - P_{PL}}{2G_{eff}} , \qquad (1)$$

where P_{PA} is the peri-airway pressure, and P_{PL} is the pleural pressure. Eqn (1) follows from Mead *et al.*(22), Lai-Fook *et al.*(19), and Fredberg and Kamm (5), where P_{PA} was referred to as the peri-bronchial pressure. In their analyses, this pressure (the pressure from the parenchyma on the outside of the airway) was found to equal the negative of the distending stress acting just outside of the airway wall from the surrounding intact parenchyma.

The mechanical fundamentals are described in Figure 4, with P_{PL} < 0 indicating a positive radial stress (τrr >0). Figure 4A demonstrates an equilibrium uniform stress state P_{PA} = P_{PL} with P_{ALV} = 0, and this defines the uniform-stress hole radius, $R_{H,U}$. In Figure 4B, a non-uniform stress is imposed by a slight change in P_{PA} so that $P_{PA} \neq P_{PL}$, and the hole radius changes to R_{H} . Eqn (1) defines the shear modulus (G) with $\frac{\Delta R}{R}$ = $(R_H - R_{H,U})/R_{H,U}$ representing the fractional change in the hole radius (R_H) from the uniform stressed state $R_{H,U}$ when P_{PL} is slightly modified.

While Figure 4 describes the situation for homogeneous alveolar pressures, we apply this approach for non-homogeneous alveolar pressures (as might occur with upstream closure), and represent the fractional change in hole radius as $\frac{\Delta R}{R} = (R_H - R_{H,E})/R_{H,E}$, where $R_{H,E}$ is the hole radius at an equilibrium state when $P_{PA} = P_{PL}$ but a fraction (fobs) of the alveolar pressures are modified from $P_{ALV} = 0$. R_H is the hole radius when $P_{PA} \neq P_{PL}$. We apply Eqn 1 to evaluate an effective shear modulus G_{eff} .

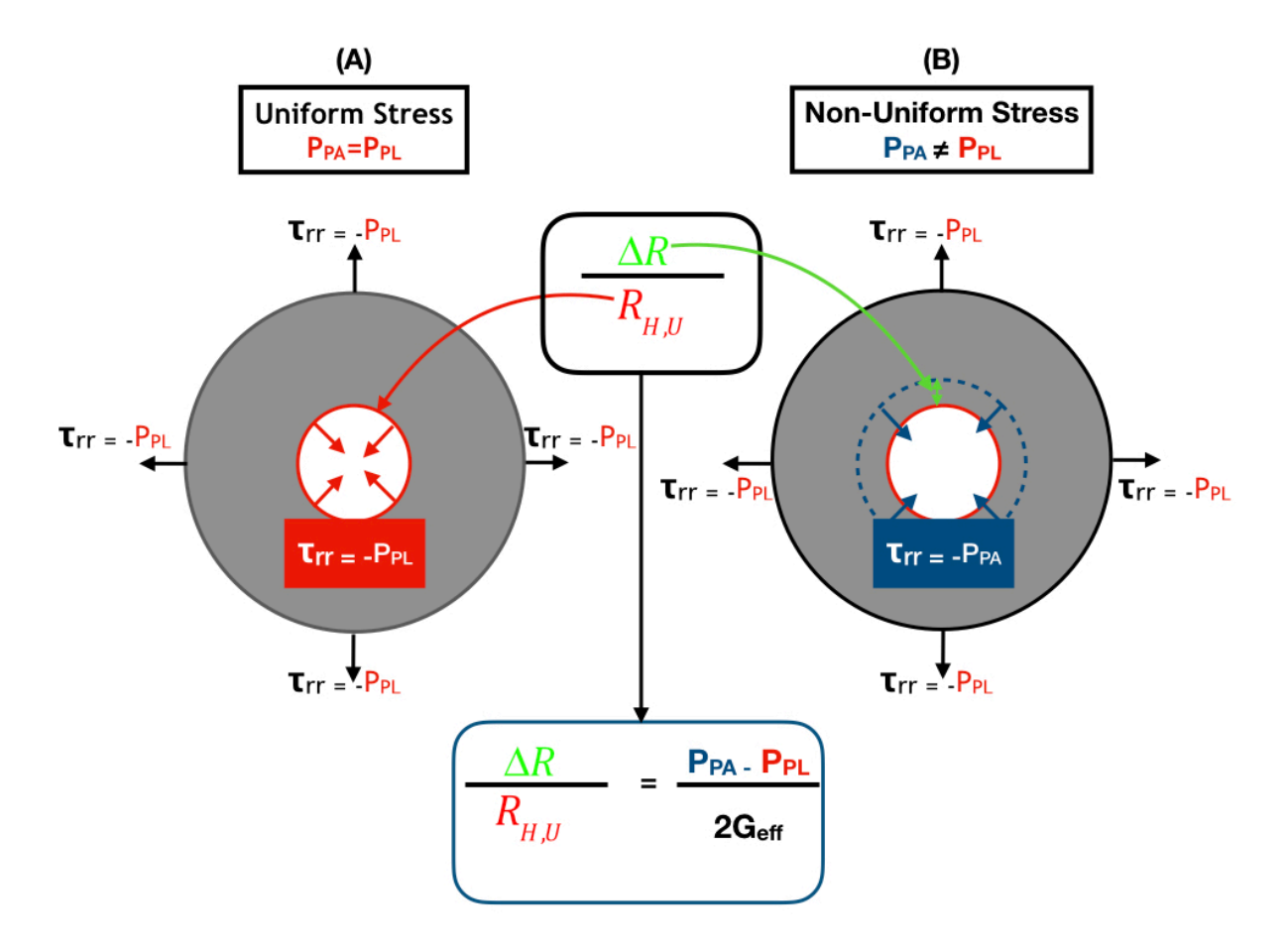


Figure 4 (A) Parenchyma in equilibrium uniform stressed state. (B) Change in hole lumen with change in peri-airway pressure, P_{PA} , from the uniform stress condition P_{PL} .

2.3. Simulation Conditions

To investigate parenchymal tethering mechanics, we conducted a series of FEM simulations in which the pressures within individual alveoli were selected randomly (using a uniform distribution) to have an internal pressure associated with: 1) a normally functioning alveolus, or 2) an obstructed alveolus. We assume that a normally functioning alveolus sustains $P_{ALV} = 0 \ cmH_2O - \text{this represents atmospheric pressure and a direct connection to the mouth in a static (breath-hold) situation. In contrast, an obstructed alveolus is set to an internal pressure of either <math>P_{OBS} = -4 \ cmH_2O$ (hypo-inflated), or $P_{OBS} = +4 \ cmH_2O$ (hyper-inflated), as explained above. For any simulation, all obstructed alveoli had the same pressure, though we

acknowledge that a distribution of inflation pressures could exist. The pleural pressure (P_{PL}) was held constant at either P_{PL} = -5 cmH₂O, -10 cmH₂O, or -15 cmH₂O. For a given P_{PL} , the stressed equilibrium state ($R_{H,E}$) was identified, and then G_{eff} , was measured by perturbing P_{PA} over the range $P_{PL} - \Delta P < P_{PA} < P_{PL} + \Delta P$, where ΔP =0.2 cmH₂O. The effective hole radius R_H was calculated by averaging the Euclidean distance from the midpoint (m_x, m_y) to each of the interior node points of the hole (x_i, y_i)

$$R_{H} = \frac{\sum_{i=1}^{(x_{N}, y_{N})} \sqrt{(x_{i} - m_{x})^{2} + (y_{i} - m_{y})^{2}}}{N}$$
 (2)

where the midpoint is the geometric center of the locus of points that describe the perimeter of the hole. The change of effective radius ΔR vs. ΔP yields the shear modulus as determined by Eqn (1).

2.3.1. Computational Costs

The models we investigate are computationally large. Two issues are prominent – 1) the total memory size, and 2) the total CPU time. Simulations were conducted on Tulane's Cypress supercomputer (based upon a Dell Z9500 with Intel Xeon E5-2680 Sandy Bridge architecture). The code was constructed in C++ and utilized the MPI library, PETSC(1) and Hypre(4) for linear algebra optimization, and ParMETIS(16) for model partitioning. Using this software/hardware combination, benchmark studies demonstrated that the total computational time was inversely related to the number of processers. Thus, our computational model was highly scalable.

The memory usage as a function of the size of the model is approximately

$$[Total Memory (MByte)] = 0.3 x [# of Alveoli] + 1500$$
(3)

Simulations were completed using two nodes, each with 20-cores.

2.3.2. Identification of R_{ROI}

To investigate the parenchymal region of interest (R_{ROI}) that defines the necessary domain size to faithfully represent the solution of an infinite domain with the same fraction of obstructed alveoli, simulations were conducted with random alveolar pressure distributions with 50% obstructed alveoli. In these calculations, the outer surface ($r = R_{OUTER}/R_H$) is modeled as being supported by the pleural pressure (following Mead). We sequentially increase R_{OUTER}/R_H to estimate the dependence of G_{eff} on the domain size for a given fraction of obstructed (unaerated) alveoli. These were studied for $2 \le \frac{R_{OUTER}}{R_H} \le 9$, with $P_{PL} = -5$ cmH₂O. To identify the statistical variance, numerical experiments were conducted with n = 5 different uniformly random distributions. R_{ROI} is identified by the percentage deviation of G_{eff} from the asymptotic value for an infinite domain, G_{∞} . Once the region of influence was established, R_{ROI} was used for all further simulations.

2.3.3. Establishment of Validity of the Random Distribution Model

To investigate the effects of localized alveolar pressure distributions for comparison with random distributions, simulations were conducted with localized obstruction distributions with the fraction of obstructed/total alveoli equal to $f_{OBS} = 0.25$, 0.5, or 0.75 through the addition of quadrants of collapsed alveoli. Likewise, simulations for uniform random distributions with equivalent f_{OBS} of were conducted. In these simulations, $P_{PL} = -5$ cmH₂O and $P_{OBS} = -2.5$ cmH₂O (hypo-inflated). We performed n=5 independent trials.

2.3.4. Parenchymal Tethering Mechanics – Evaluation of Geff

After establishing ROI, we explored the functional relationship between G_{eff} and the distribution of obstructed alveoli at specific values of P_{PL} = -5 cmH₂O, -10 cmH₂O, or -15 cmH₂O, with the fraction of obstructed/total alveoli, f_{OBS} = 0.2, 0.4, 0.6, 0.8, 1.0. Each

computational experiment was conducted with five independent trials (n = 5) to identify the statistical variance between trials.

3. Results

3.1. <u>Identification of Region of Interest</u>, R_{ROI}

We estimate the region of influence (R_{ROI}) for the parenchyma surrounding an airway by G_{eff} as a function of the domain size. From Figure 5, it is clear that G_{eff} converges to a finite value (G_{∞}) with increasing R_{ROI} , which we estimate by the non-linear regression based on the deformation of an annular disc of isotropic material:

$$G = G_{\infty} \left[1 - A \left(\frac{R_{OUTER}}{R_H} \right)^{-2} \right]. \tag{4}$$

For P_{ALV} =0, and P_{PL} =-5 cm H_2 0, we find G_{∞} = 5.836 \pm 0.015 cm H_2 0, and A = 1.153 \pm 0.02. From this result, we estimate the computational accuracy as a function of R_{OUTER}/R_H (see inset of Figure 5.

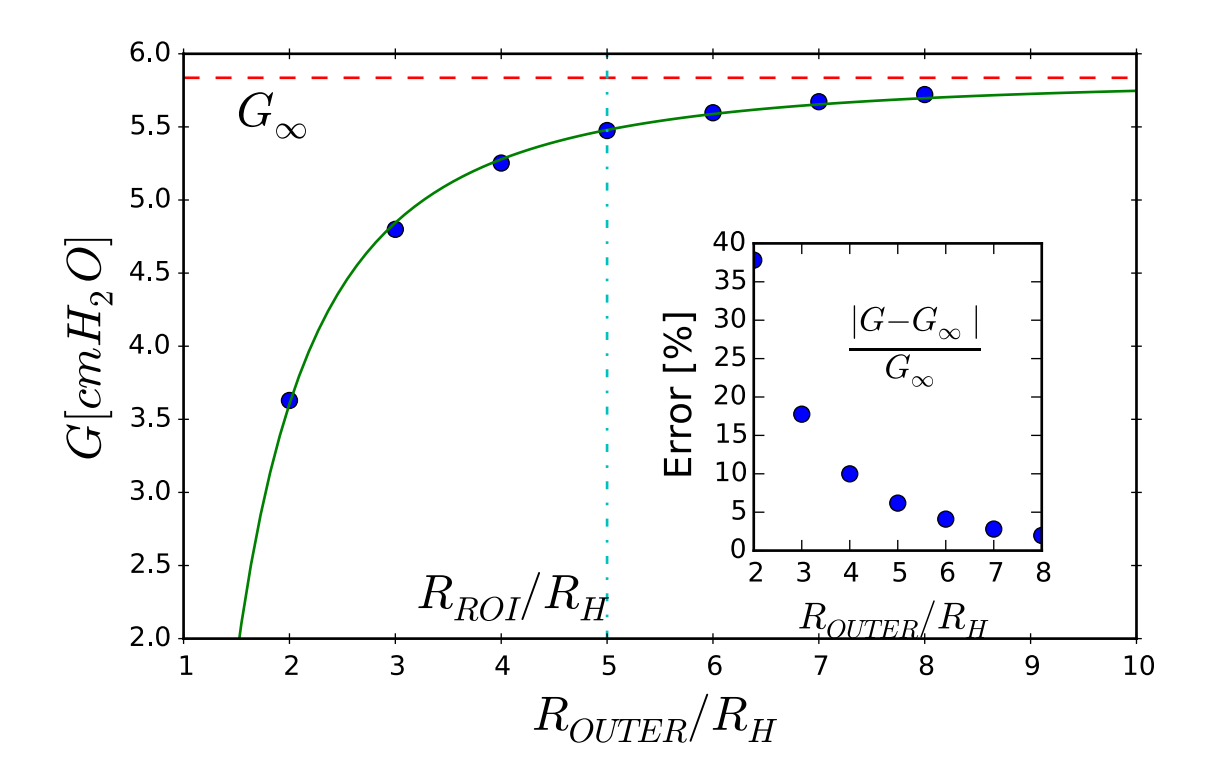


Figure 5: Calculation of the effective shear modulus, G_{eff} , as a function of the region of interest (ROI) scaled by the 'hole' radius (R_H).

In addition to accuracy, computational costs are important for considering the appropriate domain size. Table 1 presents the total memory usage and total CPU time (Total Wall Clock Time * 40 processors) for simulations as a function of the region of interest for the parenchymal domain.

R _{ROI} /R _{AW}	# of Alveoli (x10³)	Total Memory (GB)	Total CPU Time (hours)
2	6	3.4	0.3
3	17	6.6	34
4	32	11	115
5	51	17	190
6	75	24	311
7	103	32	444
8	135	42	634
9	172	53	797

Table 1: Number of alveoli, memory usage, and computational cost associated with the domain size

We identified $R_{OUTER}/R_H = 5$ as a judicious choice for the dimensionless region of influence (R_{ROI}/R_H) since it provides estimates within approximately 5% of G_∞ at a tenable computational cost. Future full-scale models of the lung could therefore use this R_{ROI} to accurately model parenchyma tethering effects surrounding collapsible airways.

The model depth (z – direction) for the ROI studies was set to 1.5 R_{H} . Further convergence analysis was conducted by evaluating G_{eff} as a function of depth. Doubling the depth resulted in only a slight increase of G_{eff} of 3.5%, and so all further calculations were conducted with the model depth equal to 1.5 R_{H} .

3.2. Establishment of the Validity of the Random Distribution Model

With R_{ROI} established, the effect of obstructed alveoli localization was examined with P_{PL} = -5 cm H_2 0, $(P_{ALV})_{OPEN}$ = 0 cm H_2 0 and P_{OBS} = -2.5 cm H_2 0. Simulations were conducted to compare G_{eff} between uniformly random distributions and localized distributions of alveoli with upstream closure. Five distinct trials with different realizations of the same uniform random distribution (n=5) were investigated to estimate the simulation variability.

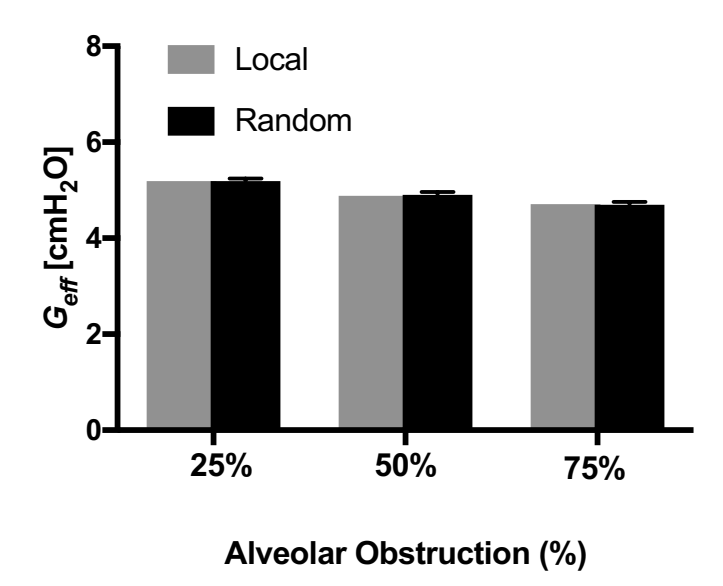


Figure 6: Comparison of localization of obstructed alveoli and heterogeneous distribution. Error bars represent the standard deviation.

These results illustrate that there is only a very small difference in G_{eff} between localized and random distribution models (<1%). A two-way ANOVA was conducted (p < 0.05) and Sidak multiple comparison tests were performed to show that there was no significant difference in G_{eff} in each group.

These results support our hypothesis that a random distribution of obstructed alveoli faithfully represents the large-scale parenchymal mechanics. In addition, the standard error is extremely small (<<1%), which further demonstrates the robustness of the random modeling approach. Since the models with localized obstructed alveoli demonstrate equivalent G_{eff} as the randomly distributed models, this justifies the use of the derived values of G_{eff} for predictions of mechanical interactions that can occur in ARDS.

3.3. Evaluation of Geff

With our two fundamental questions satisfied, we seek to explore the overall mechanical properties of systems with a subset of obstructed alveoli with P_{PL} = -5, -10, or -15 cmH₂O. We explore this behavior as a function of the transpulmonary pressure (P_{TP}), where,

 $P_{TP} = (P_{ALV})_{open} - P_{PL}$, with $(P_{ALV})_{open} = 0$, with obstructed alveoli in either the hyper-inflated state $(P_{OBS} = +4 \text{ cmH}_20)$ or hypo-inflated state $(P_{OBS} = -4 \text{ cmH}_20)$. The fraction of obstructed alveoli was varied over $0 \le f_{obs} \le 1$ in increments of 0.2.

Data from these simulations are shown in Figure 7(A) and indicate that hyper-inflated obstructed alveoli cause an increase in G_{eff} , while hypo-inflation causes a reduction of G_{eff} . The degree of change in G_{eff} is monotonically related to f_{OBS} . We note that increasing the ratio of hypo-inflated obstructed alveoli causes local distension of nearby open alveoli, which causes those alveoli to slightly stiffen. Nevertheless, the increase in hypo-inflated alveoli causes the size of the entire domain to reduce since the domain is not a fixed size (the external boundary condition is defined by P_{PL}). This results in a net softening of the parenchyma, leading to a meso-scale reduction of G_{eff} . The opposite is true for hyper-inflated alveoli, leading to a meso-scale increase of G_{eff} .

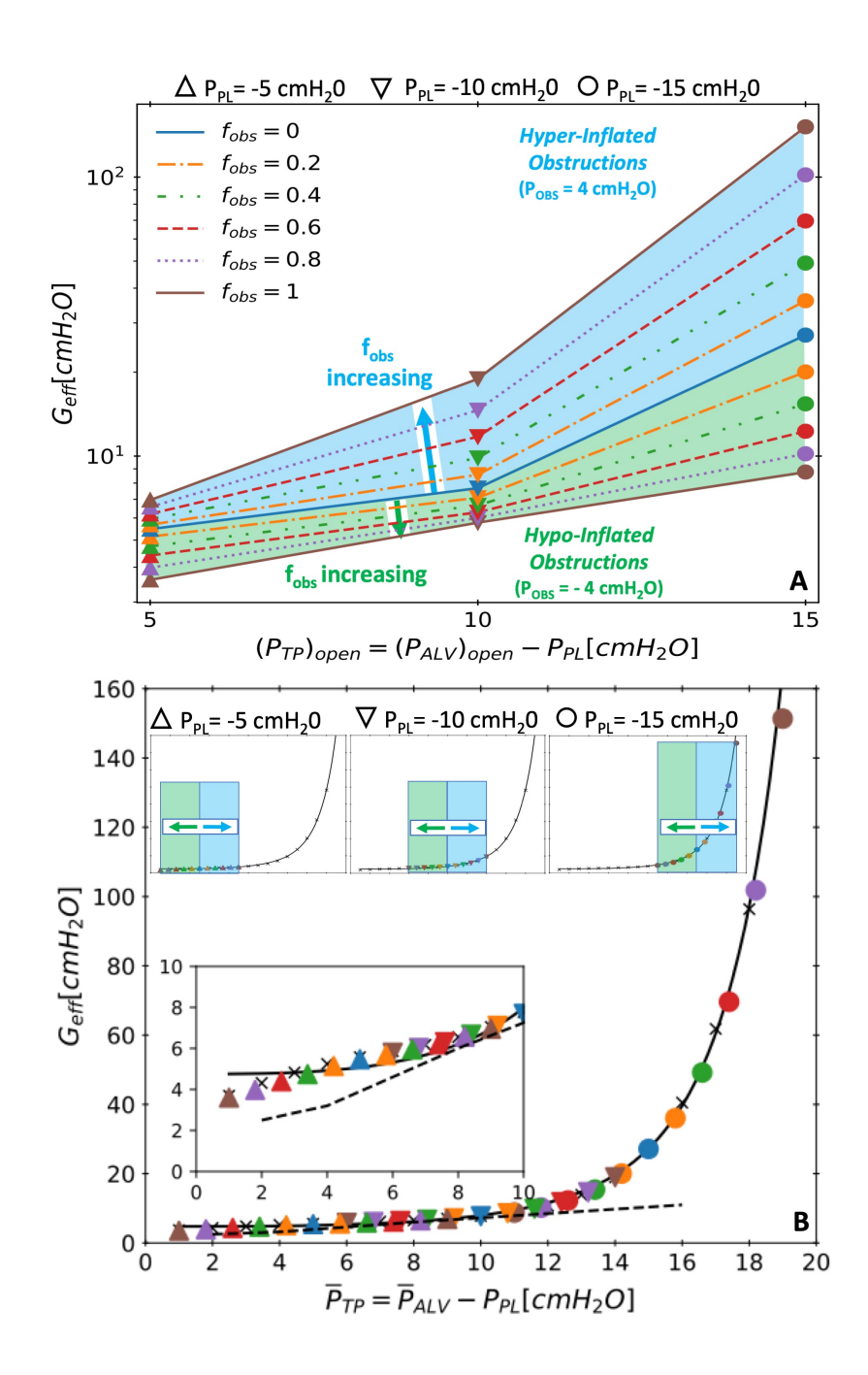


Figure 7: (A) G_{eff} as a function of P_{TP} with $(P_{ALV})_{open} = 0$, and hyper-inflated obstructed alveoli $P_{OBS} = +4$ cmH20 (shaded **blue**), or hypo-inflated obstructed alveoli $P_{OBS} = -4$ cmH20 (shaded **green**) for $P_{PL} = -5$ cmH20 (Δ), $P_{PL} = -10$ cmH20 (∇), and $P_{PL} = -15$ cmH20 (Ω). Fraction of obstructed alveoli varies over $0 \le f_{obs} \le 1$.

⁽B) G_{eff} based on the volume-average transpulmonary pressure of surrounding alveoli, which demonstrates a mastercurve. Shaded regions in sub-panels guide towards the location of hypo- and hyper-inflated data for each P_{PL}. The dashed line represents the experimental data from Lai-Fook *et al.*¹⁶

3.4. <u>Geff</u> as a Function of the Mean Alveolar Pressure

We seek a representation that will collapse the data from Figure 7A to a single relationship to facilitate incorporation into a reduced-dimension model of the lung. To explore this behavior, we investigated G_{eff} as a function of the weighted average transpulmonary pressure $(\overline{P_{TP}})$

$$\overline{P_{TP}} = \overline{P_{ALV}} - P_{PL}, \qquad (5)$$

where P_{PL} is the pleural pressure and $\overline{P_{ALV}}$ is the average of the all the alveolar pressures within the parenchyma,

$$\overline{P_{ALV}} = (1 - f_{OBS})(P_{ALV})_{open} + f_{OBS}(P_{OBS}).$$
 (6)

Figure 7B re-expresses the data from Figure 7B, demonstrating that $\overline{P_{TP}}$ effectively collapses the data to a master curve. These data were fit to an exponential function,

$$G_{eff} = A e^{b \overline{P_{TP}}^3}, (7)$$

where A = 4.75 \pm 0.12 cmH20, and B = 5.17x10⁻⁴ \pm 4.9 x10⁻⁶ cmH20⁻³, which provides a coefficient of determination of $R^2 = 0.99$.

4. Discussion

The analysis above demonstrates that a single master curve exists that can be used to estimate G_{eff} as a function of the fraction of alveoli and the pressures within obstructed and unobstructed alveoli in proximity to the airway. This result can be used to estimate the parenchymal tethering mechanics of embedded collapsed airways without resorting to a complete FEM model that would otherwise require an extraordinary computational expense (see Table 1). The meso-scale empirical behavior from these reduced-dimension results allows for

the incorporation of parenchymal mechanics into a model of a heterogeneous distribution of obstructed alveoli within the parenchyma using feasible computational resources.

Figure 7B compares our predictions of Geff to estimates from experiments by Lai-Fook et

al(19), which were conducted to analyze the mechanical properties of isolated dog lobes. These simulations demonstrate that agreement is best over the range $6 < \overline{P_{TP}} < 12 \ cmH_2O$. At smaller values of $\overline{P_{TP}}$, our simulations over-estimate Geff, though both the simulations and experiments indicate a similar reduction in slope. We speculate that our over-estimate of $G_{\rm eff}$ is due to either a surfeit of fibers over that which exists physiologically, or alveolar structural collapse that was not simulated. Our model includes a realistic reduction of surface tension with alveolar volume, and so we do not attribute the deviation to be due to surfactant effects. For $\overline{P_{TP}} > 12~cmH_2O$, the non-linear increase in $G_{\rm eff}$ results from a highly nonlinear stiffness characteristic of collagen, which becomes more significant as the pre-stress increases with $\overline{P_{TP}}$. This behavior is similar to that described by Denny and Schroter(3). In this range, the overall system may be stiffer than experimentally observed because of cross-linked fibers that exist at the faces of our alveolar elements. As described by the excellent review article by Stamenovic (28), this may explain some of the non-linear increase in G_{eff} . Furthermore, it has also been suggested by Fredberg and Kamm (5), following the work of Budiansky and Kimmel(2), that differences in micro-scale stiffness from the macro-scale could deviate in a non-affine manner as a result of structural connectedness and prestress within the structural matrix. We note that our models were developed with fiber densities following the studies of Mercer and Crapo(23). Though they were not tuned, it would be possible to change these values to better fit the experiments by Lai-Fook et al (19). Furthermore, fiber properties may change in disease, and it therefore would be valuable to predict $G_{\it eff}$ equations of state for a range of diseases from fibrosis to emphysema.

4.1. Application - Parenchymal Tethering Analysis in Simple Airway Model

To demonstrate the implementation of the reduced-dimension mechanics of the parenchyma, a simplified model was constructed with a single airway surrounded by parenchyma using the 'pig-in-a-blanket' model illustrated in Figure 8, with an airway laminated inside the parenchymal hole that was used to calculate G_{eff} .

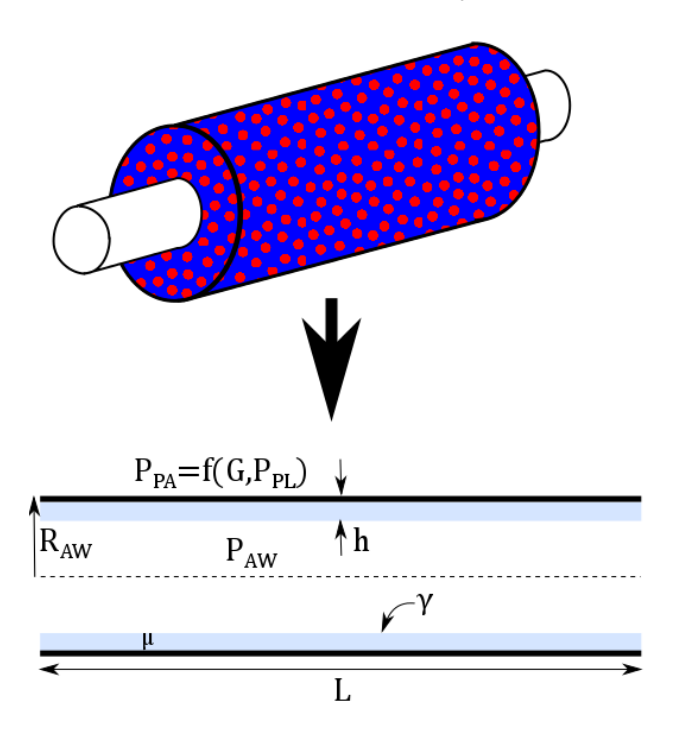


Figure 8: Simple airway model of conducting airway surrounded by parenchyma with heterogeneously distributed obstructed alveoli.

In this application, the airway transmural pressure is influenced by the peri-airway pressure induced by the parenchymal tethering mechanics, and the liquid lining that reduces the internal pressure by the Law of Laplace. This relationship is provided by

$$P_{TM} = P_{AW} - 2G_{eff}(\Delta R/R) - P_{PL} - \gamma/(R_{AW} - h)$$
(8)

where PTM is the transmural pressure, P_{AW} is the airway pressure, G_{eff} is the effective shear modulus, $\frac{\Delta R}{R} = (R_H - R_{H,E})/R_{H,E}$, P_{PL} is the pleural pressure, γ is the surface tension, and h is the liquid lining. The change in the airway radius is governed by a tube law of the form proposed

by Lambert et al.(21), and schematically illustrated in Figure 9. Additionally, this model assumes that the airway wall has no thickness, so $R_{AW} = R_H$.

A series of simulations were conducted on this single airway model following the protocol implemented by Ryans et al.(27) In this analysis we investigate only the interrelationship of the parenchymal tethering and the transmural pressure of the airway to observe the effects on airway caliber. We neglect the pressure difference between the airway and alveoli that could drive flow, and thus this is a non-equilibrium analysis.

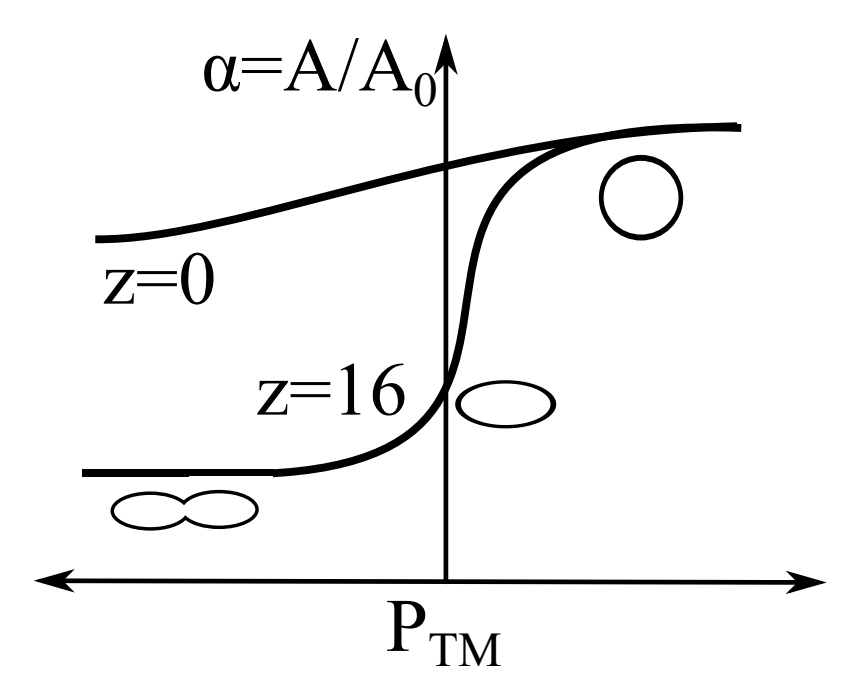


Figure 9: Tube law at the trachea (z=o) and an airway at the 16th generation (z=16).

We consider the effect of parenchymal tethering of a highly compliant 16^{th} generation airway incorporating parenchyma with ($f_{OBS} = 0$, 1) of obstructed alveoli in a hypo-inflated state, $P_{OBS} = -2.5 \text{ cmH}_20$, with $P_{PL} = -5 \text{ cmH}_20$. As a simple model of ARDS we investigate a high surface tension case with $\gamma = 50 \frac{dyn}{cm}$, and a 'wet lung' with $\left(V_{liq}/V_{AW}\right)_{min} = 0.05$, where V_{liq} and V_{AW} are the liquid lining volume and airway volume at the maximally inflated state.

 $R_{\rm AW}$ was investigated as $P_{\rm AW}$ was reduced from the maximally inflated pressure correlating to $R_{\rm AW}=R_{\rm AW,max}$. In this analysis, we predict the stability from the dimensionless liquid-lining thickness, $\varepsilon=h/R_{\rm AW}$. As the airway radius decreases with reduced $P_{\rm AW}$, h increases due to conservation of mass, and therefore ε increases. We assume that the airway becomes unstable to fluid-structure instabilities when $\varepsilon_{\rm crit}=0.12$, leading to the formation of a liquid-bridge obstruction that would cause the acinus for this airway to enter an obstructed state (9-11, 14, 15). In multiple airway systems this would, in-turn, influence $G_{\rm eff}$ for the parenchyma surrounding airways in which the R_{ROI} intersected that acinus, possibly leading to large-scale effects by reducing the tethering behavior of those airways, and so on.

Figure 10 demonstrates the airway radius under conditions of:

- a) The limiting case of a completely untethered airway;
- b) An airway surrounded by parenchyma with completely open alveoli (0% obstruction), and
- c) An airway surrounded by hypo-inflated obstructed alveoli (100% upstream obstruction, $P_{OBS} = -2.5 \text{ cmH}_20$).

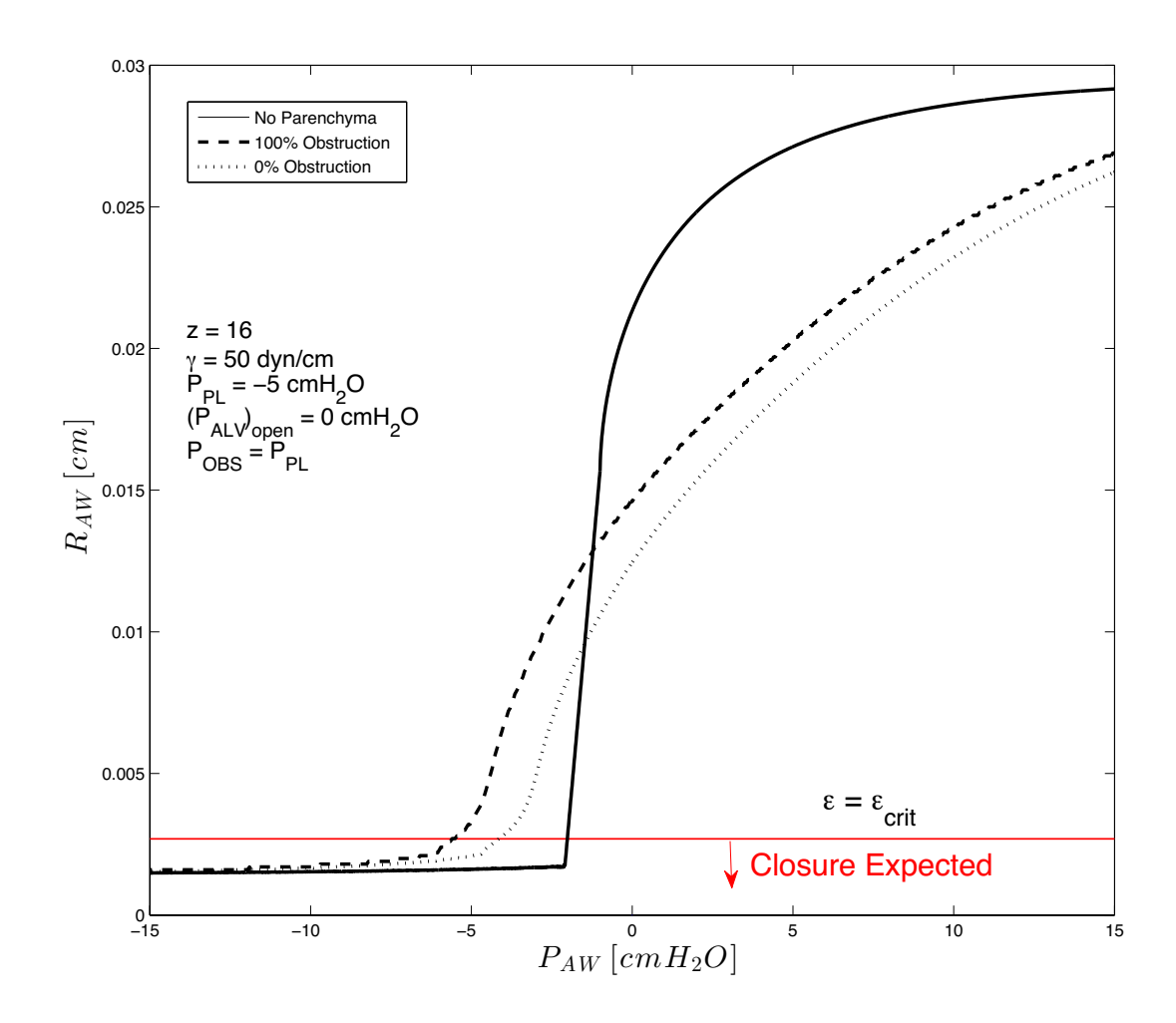


Figure 10: Simulation of a collapsible 16th generation airway without parenchymal support (solid line), with parenchymal support (dashed), and with parenchymal support from hypo-inflated obstructed alveoli (P_{OBS} = -2.5 cmH₂0, f_{OBS} =1, doted). P_{PL} = - 5 cmH₂0, γ = 50 $\frac{dyn}{cm}$.

These results show that an airway without surrounding parenchyma collapses at much greater P_{AW} than an airway surrounded by either unobstructed or obstructed alveoli. This limiting case demonstrates effects related to the complete lack of parenchyma and shows the intuitive result that an increase in P_{AW} increases stability. Following intuition, parenchyma has a stabilizing effect, with airway patency retained for $P_{AW} > -5$ cm H_2O when all alveoli are unobstructed; however, stability only exists for $P_{AW} > -3.5$ cm H_2O if all alveoli are hypo-inflated, since G_{eff} is

greater when alveoli sustain an inflated state. Interestingly, when $P_{AW} > 0 \text{ cmH}_2O$, we show that parenchyma restrains the expansion of the airway, implying that the airway is pushing against the surrounding alveoli when the non-equilibrium airway-to-alveolar pressure distribution exists.

These results demonstrate the importance of increasing P_{AW} when tethering is reduced. Positive-end-expiratory-pressure ventilation (PEEP) accomplishes this by retaining $P_{AW} > 0 \text{ cmH}_2O$, and increases the tethering effects due to an increase in G_{eff} by increasing alveolar volume. Our model predicts that the non-linear increase in G_{eff} that occurs with $\overline{P_{TP}}$ induces an added protective effect that could reduce the incidence of airway closure.

Limitations

As with all models, limitations exist owing to model assumptions. For example, we assumed that alveolar membranes that make up the parenchymal tissue act isotropically. While this is an accurate representation for uniformly inflated alveoli(30), this property is violated when collapse occurs; nevertheless, we evaluate $G_{\rm eff}$ following a continuum approach assuming perturbations from the base state. Furthermore, the lung exhibits a viscoelastic behavior(24) that is not modeled. We have also explored only a limited parameter space; when comparing randomly distributed obstructions and comparing to local distributions, we could have investigated configurations other than quadrants. Additionally, a larger range of P_{PL} and P_{OBS} could have been studied to establish the robustness of the generalization proposed herein. As described above, we ignore fluid flow and dynamic processes such as surfactant physicochemical hydrodynamics that induces hysteresis in the pressure-volume relationship that can be significant in atelectrauma and will be investigated in follow-up models. We also ignore variation in lung stiffnesses due to differences in airway wall properties – this would be incorporated through a change in the tube law demonstrated in Figure 9. We also ignore the

septal thickness associated with parenchymal tethering, which is generationally dependent. The mechanical effects of wall buckling are ignored aside from the change in area associated with the tube-law. To include buckling at the microscale is inconsistent with our reduced-dimension modeling approach.

This study only assumed that obstructed alveoli were air-filled with an upstream obstruction, and that this obstruction reduced the volume of the alveolus (hence reducing the volume of the entire model). Alternatively, these structures could be fluid filled, which would change their elastic behavior and tethering mechanics (likely increasing G_{eff}). We were also constrained to investigate alveoli that had not completely collapsed when, in fact, alveoli may collapse from low internal pressures caused by absorption atelectasis. Finally, we also note that we have investigated an idealized configuration of a compliant airway surrounded by alveoli; we have not investigated alveolar ducts, and we also assume that neighboring airways are not within the ROI.

Nevertheless, this study has demonstrated the development of multi-scale computational model of parenchyma that can be used to evaluate the meso-scale parenchymal tethering properties on highly compliant airways. Analyses of the computational data demonstrate that a single empirical relationship exists when $G_{\rm eff}$ is represented as a function of the volume-average transpulmonary pressure of the surrounding alveoli. This empirical relationship can be used to computationally model multi-scale phenomena under conditions of obstructive lung disease. These simulations could provide information related to volutrauma or atelectrauma during mechanical ventilation, and thus could help to forecast the efficacy of novel protective ventilation scenarios.

Acknowledgements

This study was supported by National Science Foundation Grant NSF CBET-1706801, National Institutes of Health Grant 1R01HL142702-01, and Research Traineeship Grant DMS-1043626. Computational resources were supported in part using high performance computing (HPC) resources and services provided by Technology Services at Tulane University, New Orleans, LA and the Louisiana Optical Network Infrastructure. We appreciate the very insightful comments by anonymous reviewers.

References

- 1. Balay S, Abhyankar S, Adams M, Brune P, Buschelman K, Dalcin L, Gropp W, Smith B, Karpeyev D, and Kaushik D. Petsc users manual revision 3.7 Argonne National Lab.(ANL), Argonne, IL (United States), 2016.
- 2. **Budiansky B, and Kimmel E**. Elastic moduli of lungs. *Journal of applied mechanics* 54: 351-358, 1987.
- 3. **Denny E, and Schroter R**. A model of non-uniform lung parenchyma distortion. *Journal of biomechanics* 39: 652-663, 2006.
- 4. **Falgout RD, and Yang UM**. hypre: A library of high performance preconditioners. In: *International Conference on Computational Science*Springer, 2002, p. 632-641.
- 5. **Fredberg JJ, and Kamm RD**. Stress transmission in the lung: pathways from organ to molecule. *Annu Rev Physiol* 68: 507-541, 2006.
- 6. **Fujioka H, Halpern D, and Gaver DP, 3rd**. A model of surfactant-induced surface tension effects on the parenchymal tethering of pulmonary airways. *J Biomech* 46: 319-328, 2013.
- 7. **Fujioka H, Halpern D, Ryans J, and Gaver III DP**. Reduced-dimension model of liquid plug propagation in tubes. *Physical Review Fluids* 1: 053201, 2016.
- 8. **Gaver III DP, Samsel RW, and Solway J**. Effects of surface tension and viscosity on airway reopening. *Journal of Applied Physiology* 69: 74-85, 1990.
- 9. **Grotberg JB, and Jensen OE**. Biofluid mechanics in flexible tubes. *Annu Rev Fluid Mech* 36: 121-147, 2004.
- 10. **Halpern D, and Grotberg J**. Fluid-elastic instabilities of liquid-lined flexible tubes. *Journal of Fluid Mechanics* 244: 615-632, 1992.
- 11. **Hammond P**. Nonlinear adjustment of a thin annular film of viscous fluid surrounding a thread of another within a circular cylindrical pipe. *Journal of fluid Mechanics* 137: 363-384, 1983.
- 12. **Higuita-Castro N, Mihai C, Hansford DJ, and Ghadiali SN**. Influence of airway wall compliance on epithelial cell injury and adhesion during interfacial flows. *J Appl Physiol (1985)* 117: 1231-1242, 2014.
- 13. Jain SV, Kollisch-Singule M, Satalin J, Searles Q, Dombert L, Abdel-Razek O, Yepuri N, Leonard A, Gruessner A, and Andrews P. The role of high airway pressure and dynamic strain on ventilator-induced lung injury in a heterogeneous acute lung injury model. *Intensive care medicine experimental* 5: 25, 2017.
- 14. **Johnson M, Kamm RD, Ho LW, Shapiro A, and Pedley T**. The nonlinear growth of surface-tension-driven instabilities of a thin annular film. *Journal of Fluid Mechanics* 233: 141-156, 1991.
- 15. **Kamm R, and Schroter R**. Is airway closure caused by a liquid film instability? *Respiration physiology* 75: 141-156, 1989.
- 16. **Karypis G, Schloegel K, and Kumar V**. Parmetis: Parallel graph partitioning and sparse matrix ordering library.
- 17. **Khan MA, Ellis R, Inman MD, Bates JH, Sanderson MJ, and Janssen LJ**. Influence of airway wall stiffness and parenchymal tethering on the dynamics of bronchoconstriction. *American Journal of Physiology-Lung Cellular and Molecular Physiology* 299: L98-L108, 2010.
- 18. **Krueger MA, and Gaver III DP**. A theoretical model of pulmonary surfactant multilayer collapse under oscillating area conditions. *Journal of Colloidal and Interface Science* 229: 353-364. 2000.
- 19. **Lai-Fook SJ, Hyatt RE, and Rodarte JR**. Effect of parenchymal shear modulus and lung volume on bronchial pressure-diameter behavior. *Journal of applied physiology* 44: 859-868, 1978.

- 20. **Lai-Fook SJ**, **Hyatt RE**, **Rodarte JR**, **and Wilson TA**. Behavior of artificially produced holes in lung parenchyma. *Journal of Applied Physiology* 43: 648-655, 1977.
- 21. **Lambert RK, Wilson TA, Hyatt RE, and Rodarte JR**. A computational model for expiratory flow. *J Appl Physiol Respir Environ Exerc Physiol* 52: 44-56, 1982.
- 22. **Mead J, Takishima T, and Leith D**. Stress distribution in lungs: a model of pulmonary elasticity. *Journal of applied physiology* 28: 596-608, 1970.
- 23. **Mercer RR, and Crapo J**. Spatial distribution of collagen and elastin fibers in the lungs. *Journal of Applied Physiology* 69: 756-765, 1990.
- 24. **Navajas D, Maksym GN, and Bates J**. Dynamic viscoelastic nonlinearity of lung parenchymal tissue. *Journal of Applied Physiology* 79: 348-356, 1995.
- 25. **Perun ML, and Gaver D**. Interaction between airway lining fluid forces and parenchymal tethering during pulmonary airway reopening. *Journal of Applied Physiology* 79: 1717-1728, 1995.
- 26. **Perun ML, and Gaver III DP**. The interaction between airway lining fluid forces and parenchymal tethering during pulmonary airway reopening. *Journal of Applied Physiology* 75: 1717-1728, 1995.
- 27. **Ryans J, Fujioka H, Halpern D, and Gaver DP**. Reduced-dimension modeling approach for simulating recruitment/de-recruitment dynamics in the lung. *Annals of biomedical engineering* 44: 3619-3631, 2016.
- 28. **Stamenovic D**. Micromechanical foundations of pulmonary elasticity. *Physiological Reviews* 70: 1117-1134, 1990.
- 29. Venegas JG, Winkler T, Musch G, Melo MFV, Layfield D, Tgavalekos N, Fischman AJ, Callahan RJ, Bellani G, and Harris RS. Self-organized patchiness in asthma as a prelude to catastrophic shifts. *Nature* 434: 777-782, 2005.
- 30. **Wilson TA**. A continuum analysis of a two-dimensional mechanical model of the lung parenchyma. *Journal of applied physiology* 33: 472-478, 1972.
- 31. **Yap D, Liebkemann W, Solway J, and Gaver Dr**. Influences of parenchymal tethering on the reopening of closed pulmonary airways. *Journal of Applied Physiology* 76: 2095-2105, 1994.
- 32. **Yap DYK, Liebkemann WD, Solway J, and Gaver III DP**. The influence of parenchymal tethering on the reopening of closed pulmonary airways. *Journal of Applied Physiology* 76: 2095-2105, 1994.

Table of Figures

- Figure 1: Representative illustration of airway obstruction resulting in the presence of aerated (blue) and obstructed (red) alveoli surrounding separate conducting airways.
- Figure 2: Approximation of heterogeneous tethering using a uniformly random distribution of obstructed alveoli ('sprinkled donut').
- Figure 3: Boundary conditions of FEM model on the fixed face (red), cylindrical face (blue), and free-moving face (green). The interior hole is assumed to be at a constant pressure (PPA) as shown in Figure 4.
- Figure 4 (A) Parenchyma in equilibrium uniform stressed state. (B) Change in hole lumen with change in peri-airway pressure, P_{PA} , from the uniform stress condition P_{PL} .
- Figure 5: Calculation of the effective shear modulus, G_{eff} , as a function of the region of interest (ROI) scaled by the 'hole' radius (R_H).
- Figure 6: Comparison of localization of obstructed alveoli and heterogeneous distribution. Error bars represent the standard deviation.
- Figure 7: (A) G_{eff} as a function of P_{TP} with $(P_{ALV})_{open} = 0$, and hyper-inflated obstructed alveoli $P_{OBS} = +4 \text{cmH20}$ (shaded blue), or hypo-inflated obstructed alveoli $P_{OBS} = -4 \text{cmH20}$ (shaded green) for $P_{PL} = -5 \text{cmH20}$ (Δ), $P_{PL} = -10 \text{cmH20}$ (∇), and $P_{PL} = -15 \text{cmH20}$ (Ω). Fraction of obstructed alveoli varies over $0 \le \text{fobs} \le 1$.
- Figure 8: Simple airway model of conducting airway surrounded by parenchyma with heterogeneously distributed obstructed alveoli.
- Figure 9: Tube law at the trachea (z=o) and an airway at the 16th generation (z=16).
- Figure 10: Simulation of a collapsible 16^{th} generation airway without parenchymal support (solid line), with parenchymal support (dashed), and with parenchymal support from hypo-inflated obstructed alveoli ($P_{OBS} = -2.5 \text{ cmH}_20$, $f_{OBS} = 1$, doted). $P_{PL} = -5 \text{ cmH}_20$, $\gamma = 50 \text{ mN/m}$.